JOURNAL OF THERMOPHYSICS AND HEAT TRANSFER
Vol. 12, No. 4, October–December 1998

Evaluation of Estimation Methods for High Unsteady Heat Fluxes from Surface Measurements

D. Greg Walker* and Elaine P. Scott†
Virginia Polytechnic Institute and State University, Blacksburg, Virginia 24061-0238

Shock interactions such as those that occur during atmospheric re-entry can produce extreme thermal loads on aerospace structures. These interactions are reproduced experimentally in hypersonic wind tunnels to study how the flow structures relate to the deleterious heat fluxes. In these studies, the fluid jets created by shock interactions impinge on a test cylinder, where the temperature resulting from the heat flux is measured. These measurements are used to estimate the heat flux on the surface as a result of the shock interactions. Finding the boundary flux from discrete unsteady temperature measurements is characterized by instabilities in the solution. The purpose of this work is to evaluate existing methodologies for the determination of the unsteady heat flux and to introduce a new approach based on an inverse technique. The performance of these methods is measured in terms of accuracy and their ability to handle inherently unstable or highly dynamic data such as step fluxes and high-frequency oscillating fluxes. The inverse methods proved to be the most accurate and stable of the methods examined.

Nomenclature

c_p = specific heat, kJ/kg K
H = order of regularization matrix, dimensionless
k = thermal conductivity, W/m K
q = integrated heat flux, W s/m^2
$\dot{q}$ = heat flux, W/m^2
S = objective function
T = calculated temperature, K
t = time, s
x = space coordinate, m
Y = measured temperature, K
α = regularization parameter, K^2 m^4/W^2
β' = variable property correction factor, 1/K
Δx = distance between nodes, m
η = transformed coordinate, dimensionless
κ = thermal diffusivity, m^2/s
ρ = density, kg/m^3
ϕ = Kirchoff temperature, K
Ψ^{-1} = matrix of measurement variances, 1/K^2

Subscripts
n = time step
0 = nominal value

I. Introduction

EXTREMELY high heat fluxes can be created by shock interactions during atmospheric re-entry of aerospace vehicles. The fluxes can be large enough to damage re-entry vehicles by imposing tremendous thermal stresses on the structures.[1–3] This phenomenon can be simulated experimentally to obtain a better understanding of the behavior of the nonuniform unsteady heat fluxes created in extreme thermal environments.[4–6]

High heat fluxes such as those that occur in shock interactions are typically evaluated by measuring the temperature on the surface of a model and employing a data reduction scheme to convert these temperatures to a corresponding flux. Two examples of facilities where measured temperatures and data reduction schemes are used to evaluate incident heating rates are described by Holden et al.[7] and Berry and Nowak.[8] Many different methodologies have been proposed to solve this type of data reduction problem, and some are outlined by Seymour.[9] It is difficult, however, to evaluate the validity of different data reduction schemes using experimental data because little is known about the nature of the actual flux.

The problem of data reduction is typically plagued by unstable solutions brought about by inherent mathematical instabilities of ill-posed problems and exaggerated by measurement errors. This can be demonstrated by examining the relationship between the measured temperature and the surface heat flux. The conventional temperature solution to conduction through a model can be expressed as some integral of the boundary flux. Attempting to find the kernel of this integral (the boundary flux) we introduce some mathematical uncertainty.[10] In other words, there is no unique solution to the problem because the data are recorded at discrete times. Furthermore, the surface flux is obtained through a differentiation of the temperature distribution in this case; the fact that we have to take a derivative sensitizes the solution to any uncertainty we have in the numerical solution, the measurement of the temperatures, the variation of the properties, or any other parameter associated with the experiment or the modeling.[11] These effects become even more significant when dealing with high heat fluxes such as those associated with shock interactions because the gradients are extremely steep and, therefore, more difficult to resolve.

There are two objectives of this work. Firstly, we want to establish when and the reason why conventional heat-flux estimation techniques fail. Secondly, we want to introduce the inverse approach as a more accurate and stable mechanism for estimating heat fluxes, particularly in situations that cannot be handled adequately by traditional methods.

II. Overview of Estimation Methods

The data reduction methods can be grouped into three primary classes. The first class is restricted to analytical techniques where a closed-form solution to the conduction equation is necessary. The second class consists of direct numerical techniques that allow increased flexibility in solving the conduction equation, but introduce additional uncertainties. The

Received Dec. 16, 1996; revision received March 11, 1998; accepted for publication March 16, 1998.

*Graduate Research Assistant, Department of Mechanical Engineering.

†Associate Professor, Department of Mechanical Engineering.

third class is made up of the proposed inverse solution techniques that address the stability issues and provide more robust solution procedures. Overviews of each method are given here, but the reader should consult the references for a detailed description of the solution methodologies.

A. Class 1 Methods

To obtain an analytic solution for the boundary flux we must first relate temperature to an arbitrary flux using the conduction equation. The temperature solution is then a function of time, space, and the unknown flux. To obtain the closed-form temperature solution necessary for class 1 methods, we must require the boundary flux to be piecewise constant, and we must assume that the properties are constant. Now the unknown boundary flux can be found as a function of the known discrete temperature measurements.

1. *Cook–Felderman (Class 1)*

An analytical solution, typical of class 1 methods, was first described by Vidal[12] and derived by Schultz and Jones.[13] A closed-form solution to the one-dimensional conduction equation with a specified boundary flux can be formulated assuming constant thermal properties. When we assume the estimated flux to be constant between temperature measurements, we can use Duhamel's theorem to obtain a surface temperature as a function of time. The unknown flux is then resolved as a function of the known temperature measurements as given by

$$q''_{0n} = \frac{2\sqrt{\rho c_p k}}{\sqrt{\pi}} \sum_{j=1}^{n} \frac{Y_j - Y_{j-1}}{\sqrt{t_n - t_j} + \sqrt{t_n - t_{j-1}}} \tag{1}$$

Note that the properties (ρ, c_p, and k) are evaluated at some nominal temperature (usually the initial temperature). This procedure (called the Cook–Felderman technique) is outlined by Cook and Felderman[14] and summarized by Seymour.[9] Cook[15] has since suggested that a correction factor can be added to the estimate to account for temperature-dependent properties, and this approach has been used with some success.[16] The flux corrected for temperature-dependent properties by β' is then given as

$$q''_n = q''_{0n}[1 + \beta'(Y_n - Y_0)] \tag{2}$$

where β' is generally a function of Y_n.

2. *Kendall–Dixon (Class 1)*

Kendall and Dixon[17] suggested a variation on the derivation of the Cook–Felderman method to help smooth the inherent instabilities in the solution. In this method, referred to as Kendall–Dixon, the temperature is integrated over time to obtain the cumulative energy into the system, and then this quantity is differentiated with a high-order, central-differencing scheme. Thus, the cumulative energy at the nth time step is

$$q_{0n} = \frac{\sqrt{\rho c_p k}}{\sqrt{\pi}} \sum_{j=1}^{n} \frac{Y_j + Y_{j-1}}{\sqrt{t_n - t_j} + \sqrt{t_n - t_{j-1}}} \Delta t \tag{3}$$

The differencing scheme suggested by Hedlund et al.[18] and then Hollis[16] to convert the quantity q_{0n} to a heat flux is

$$q''_{0n} = \frac{-2q_{n-8} - q_{n-4} + q_{n+4} + 2q_{n+8}}{40\Delta t} \tag{4}$$

and the temperature-dependent correction is the same as in Eq. (2). Because of the broad differencing scheme, this method should not exhibit sensitivity to abrupt temperature changes, and should not resolve high-frequency components of the boundary flux as well.

B. Class 2 Methods

In response to the primary drawbacks of class 1 methods, i.e., the restrictions on the functional form of the boundary flux and the constant property assumption, the trend has been to use numerical schemes rather than analytical schemes to resolve the temperature distribution. Class 2 methods are therefore characterized by the use of the measured temperature as the surface boundary condition. The methods in this classification simply require finding a discretized derivative of the temperature distribution at the surface to obtain a flux.

1. *Finite Difference (Class 2)*

The most straightforward implementation of the class 2 methods is the finite difference scheme. As in all cases, the measured temperature is the surface condition used to calculate the temperature distribution from the conduction equation given by

$$\frac{\partial}{\partial x}\left[k(T)\frac{\partial T}{\partial x}\right] = \frac{1}{\rho c_p(T)}\frac{\partial T}{\partial t} \tag{5a}$$

$$T(t = 0) = T_0 \tag{5b}$$

$$T(x = 0,\ t = t_n) = Y_n \tag{5c}$$

$$T(x = \infty) = T_0 \tag{5d}$$

Note that either a finite difference or a finite element solution technique can be used, and they will ideally result in the same temperatures at the given nodes.

Once the temperature distribution is known, the flux can be found by performing an energy balance at the surface control volume and solving for the surface flux. Normally the surface flux is calculated using Fourier's law; note, however, that in a discrete sense, the formulation must include the storage term of the surface control volume. The formulation is then written as

$$q'' = \frac{\Delta x}{2}\rho c_p \frac{\partial T}{\partial t} + \left(-k\frac{\partial T}{\partial x}\right) \tag{6}$$

where the first term represents the storage of the control volume, and the second term is Fourier's law at the interior surface of the control volume. Note that careful consideration must be given to the differencing scheme; the same scheme that was used to find the distribution must be used to discretize Eq. (6) as well. Cook[19] first suggested an explicit formulation, whereas, an implicit formulation is used here because of enhanced stability and accuracy as suggested by Patankar.[20]

Note that the finite difference method has not been formally described or examined in the literature for this application because it is merely an extension of a numerical conduction problem.

2. *Simple Implicit (Class 2)*

Holden et al.[7] reported that many techniques are not able to resolve high-frequency components of the estimated flux. This drawback gave rise to what is called the simple implicit technique. It has been found that the conduction equation cast into its Kirchoff form and discretized implicitly is able to resolve the flux at early times (with appropriate gridding) while adequately estimating high-frequency components at later times. The difference formulation is given as

$$\frac{\phi_i^{n+1} - \phi_i^n}{t_{n+1} - t_n} = \kappa(x_i, t_n)\frac{\phi_{i+1}^{n+1} - 2\phi_i^{n+1} + \phi_{i-1}^{n+1}}{\Delta x^2} \tag{7}$$

where the Kirchoff temperature is given as

$$\phi = \int_{T_0}^{T} \frac{k(T)}{k_0}\,dT \tag{8}$$

This method allows for relatively simple implementation of nonuniform gridding schemes and linearizes nonlinear problems. Also because we now are concerned with temperature averages (ϕ) rather than the actual temperatures, the transformation reduces the impact of steep gradients for both linear and nonlinear cases. However, the surface derivative is still sensitive to measurement errors. Furthermore, the standard method of flux estimation from the distribution is to simply take the derivative at the surface. This route however, ignores the energy stored in the surface control volume as described earlier in Eq. (6).

3. Rae–Taubee (Class 2)

Another particularly successful finite difference method that has been well documented is the Rae–Taubee technique. First described by Dunn et al.[21] and summarized by Glass,[22] the conduction equation is transformed into a quasilinear differential equation using Kirchoff's transformation [Eq. (8)]. The method is then further refined by scaling the spatial dimension by the penetration depth to obtain a new coordinate, η, where

$$\eta = x/2\sqrt{\kappa_0 t} \tag{9}$$

The spatial domain now changes with time and follows the penetration depth of the total added energy. The obvious advantage of this feature is an increase in the resolution of the temperature distribution at early time steps, which allows more accurate estimation of the steep slopes and small depths associated with high heat fluxes. The conduction equation is now written as

$$\frac{\kappa}{\kappa_0}\frac{\partial^2\phi}{\partial\eta^2} + 2\eta\frac{\partial\phi}{\partial\eta} = 4t\frac{\partial\phi}{\partial t} \tag{10a}$$

$$\phi(t = 0) = 0 \tag{10b}$$

$$\phi(\eta = 0,\ t = t_n) = \int_{Y_0}^{Y_n} dT \tag{10c}$$

$$\phi(\eta = 5) = 0 \tag{10d}$$

where the formulation is in terms of the Kirchoff temperature defined in Eq. (8). To maintain a semi-infinite slab assumption, the temperature at five penetration depths ($\eta = 5$) is zero. Note that temperature-dependent properties can be incorporated into the model with this method.

As Holden and Kolly[23] point out, the scheme is convenient because regridding is automatic. George et al.[24] performed an evaluation of this technique compared to previously known methods. They found that the Rae–Taubee technique could resolve early heat flux as well or better than other schemes. Note, however, that the Rae–Taubee technique suffers from inadequate grid spacing at later times. Furthermore, the Rae–Taubee method also does not account for the energy-stored term in the surface control volume. Therefore, we see less agreement at later times because of the increasing size of the control volume.

C. Class 3 Methods

The third class of methods, characterized by inverse heat conduction procedures, is new to this application.[25] Although the problem under consideration is not a true inverse problem because the temperature measurements are on the surface of the model, an inverse technique based on a least-squares minimization is being proposed because of the high uncertainties in the measured temperatures and inherent instabilities in the problem.

The solution is found by first calculating surface temperatures from an initially assumed heat flux. This forward temperature solution can be found by any appropriate conduction solution method such as a finite element that can include temperature-dependent properties. Note that this feature also makes multidimensional analysis possible; therefore, another obvious advantage of the inverse technique is the ability to resolve lateral conduction effects that will not be discussed in this work. The calculated temperatures from the forward-conduction analysis are then compared to the measured temperatures in a least-squares sense. An appropriate optimization scheme can then be used to find an updated guess by minimizing an objective function that involves the difference between calculated and measured temperatures. This procedure avoids differentiating the distribution at the surface, reducing the amplification of uncertainty inherent in direct techniques.

1. Regularization (Class 3)

The objective function for the first of the class-3 techniques is formulated by introducing a regularization term to a sum of squares of the temperature differences and is given by

$$S = [T(q) - Y]^T\Psi^{-1}[T(q) - Y] + \alpha(Hq)^T\Psi^{-1}(Hq) \tag{11}$$

where the regularization term is $\alpha(Hq)^T(Hq)$. This formulation is typical for true inverse problems and is referred to as the "regularization" technique. The formulation follows that of Tikhonov and Arsenin,[26] except that the matrix of measurement variances (Ψ^{-1}) has been included as described by Beck et al.,[10] i.e., the simplest formulation is $\Psi = \sigma^2 I$. In our case, first-order regularization is used ($H = H_1$), which limits the flux gradients. That is, H_1 contains the coefficients of a first-order finite difference scheme as shown by Beck et al. The matrix (in compact form) becomes

$$H_{ij} = \begin{cases} 1 & \text{if } j = i \\ -1 & \text{if } j = i + 1 \\ 0 & \text{otherwise} \end{cases} \tag{12}$$

The calculated temperatures, $T(q)$, in Eq. (11) can be obtained by any appropriate forward-conduction solution. As a result we can incorporate temperature-dependent properties that cause the solution to become nonlinear. Because of this nonlinearity, the solution ($q = q_0 + \Delta q$), where q_0 is the flux estimate at the previous iteration, is formulated in terms of a flux correction Δq. By defining the calculated temperature as the first term of a Fourier series ($T = T_0 + X\Delta q$), where T_0 is the temperature resulting from q_0, and X is the sensitivity matrix. The coefficients of this matrix are defined as

$$X_{ij} = \left.\frac{\partial T_i}{\partial q_j}\right|_{q_0} \tag{13}$$

a linear set of equations can be obtained by equating the differentiated objective function to zero. Thus, Δq can be found from

$$\Delta q = [X^T\Psi^{-1}X + \alpha H^T H]^{-1}[X^T\Psi^{-1}(Y - T_0) - \alpha H^T H q_0] \tag{14}$$

The flux estimate is found iteratively by calculating the flux correction based on an initial guess and updating the guess until the correction is arbitrarily small.

Note that we must examine several time steps simultaneously to achieve stabilization through the use of regularization. A sequential approach where a minimum number of future time steps is examined at once is the most efficient. Generally, for a sequential solution approach (which was used here), the minimum number of required time steps depends on the order of regularization. In our case, which uses first-order regularization suggested by Scott and Beck,[27] the minimum required number of time steps is two. Note that more than two steps introduced too much error into our solution. A rough guess of

the regularization parameter can be determined based on the variance of the error in the measured data as $\alpha = (\sigma_y/q_n)^2$. The optimal regularization parameter can also be found through trial and error by requiring the objective function value S, to be on the same order of magnitude as the experimental noise. A value of $\alpha = 0.00001\ K^2\ m^4/W^2$ was found to satisfy both approaches to determining the regularization parameter.

The regularization technique exhibits several features not found in the other classes of solution methods. Firstly, we can include information about nonconstant variance of the measurement errors in the Ψ^{-1} matrix. Because the method is statistical in nature, we can mitigate the influence of noisy data. Also, because we are not taking derivatives of the temperature distribution, small errors tend to not become amplified in the solution as in the other methods. Finally, multidimensional problems can be considered as mentioned previously.

2. Explicit Regularization (Class 3)

Contrary to a formal regularization formulation, we realize that future time steps are unnecessary because the temperature response to a changing flux is (theoretically) instantaneous at the surface. Furthermore, the relatively high sensitivities allow us to reduce the influence of the regularization term by eliminating the future times. This modified regularization technique will be called the "explicit regularization" method. The objective function given by Eq. (11) will be written in terms of the current time step and the previous estimate that results in a scalar equation. Thus, with first-order regularization, the modified objective function becomes

$$S = (Y_i - T_i)^2 + \alpha(q_i - q_{i-1})^2 \tag{15}$$

where q_{i-1} is the previous estimate that is somewhat different than the regularization that was used previously. We can explicitly solve for the flux correction as we did for Eq. (14) to obtain

$$\Delta q = \frac{X(Y_i - T_{0i}) + \alpha(q_{0i} - q_{i-1})}{X^2 - \alpha} \tag{16}$$

Notice that if the regularization were turned off, i.e., the regularization parameter is set to zero, we are left with an exact matching technique. This explicit regularization technique is also extremely fast because we can solve for the flux sequentially without having to invert a matrix.

To the knowledge of the authors, this method has not been previously described because typical inverse methods require more smoothing than our case. We have retained the ability to damp noise but have not limited ourselves by requiring smoothing over several time steps to maintain stability.

III. Analysis

The canonical experiment by Holden et al.[7] was used as a baseline for generating the test cases to be examined. The published data for a single sensor (HT_37 in Fig. 1) contain 20 ms of measurements at a sampling rate of 20 kHz with a start up period of approximately 6 ms. The visible fluctuations are actually a result of flow conditions and need to be resolved. The sudden jump in temperature as well as the dynamic nature were among the features being simulated.

Because we do not know the flux in a real case, it is difficult to determine the accuracy of any given method. Therefore, to find the performance characteristics of each estimation method, simulated data that mimic shock-tunnel measurements were generated from predetermined heat fluxes. These test cases include a step flux, a pulse flux, and a temperature spike (common among inverse evaluations), as well as high-frequency oscillating fluxes (to characterize the unsteady nature of the real data). In all test cases a nominal heat flux of 1135 W/cm^2 (1000 Btu/ft^2 s) was used to simulate the real heat fluxes. The

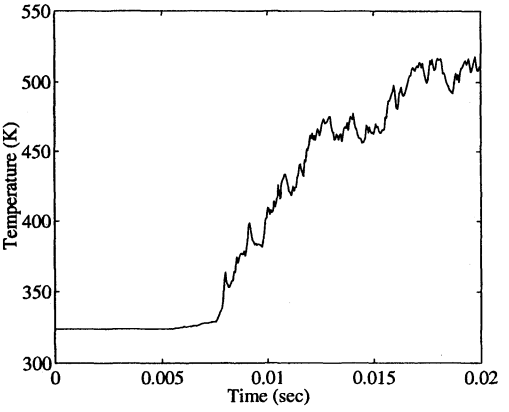

Fig. 1 Surface temperature measurements from gauge HT_37 in run 85 typify the temperature range and unsteady signals that are being examined.

simulated temperature data were obtained from the predetermined heat fluxes via a finite element conduction solution that included temperature-dependent properties of Pyrex®. To model the experimental noise of thin film temperature sensors, a normally distributed random error of 0.32 K^2 (1.0 R^2) variance was added to the indicated data sets.

It has become standard practice within the inverse community, as outlined by Beck,[28] to use test cases in which a heat flux function is defined and then estimated using simulated data to evaluate the behavior of a method. Murio[29] suggests that one of the advantages of evaluating methods in this way is that it allows for the appropriate evaluation of parameters involved in the estimation. Each of the test cases is outlined next.

1) Step flux: In a discrete sense, the step change in flux represents a large, sudden change in the heat rate. This type of flux can be found immediately following a 3-ms startup period when the flow first impinges the model. Because this type of heat flux is usually found at the beginning of experiments, it is important to determine what effect this characteristic might have on downstream estimates as well as determine the behavior of the estimates during a constant flux after the step. The hypothetical flux is zero until 3 ms where it jumps to 1135 W/cm^2 (1000 Btu/ft^2 s). The flux is then set back to zero at 7 ms. The features highlighted by these data include large temperature changes and constant flux conditions.

2) Pulse flux: This type of test case does not model any specific physical phenomenon, but should provide insight into the behavior of the estimation routines at large singular fluctuations. This type of estimation also provides insight into the level of stabilization added to the solution. The data consist of a single heat flux data point of 1135 W/cm^2 (1000 Btu/ft^2 s) midway through the data region.

3) Temperature spike: We can simulate experimental errors such as electrical pulses recorded by acquisition facilities that fall outside the normal range of experimental noise. An example of this behavior was recorded at GASL,[30] when Schlieren photographs caused an errant spike with an order of magnitude greater than the nominal experimental noise. For this test case, the temperature produced by the pulse is treated as an error in temperature measurement. In other words, the flux is zero but we retain the temperature signature at the point of the spike as if the flux did exist. With this test case, the effects of anomalistic measurements on the data reduction can be studied as well as the effects of measurement noise.

4) High-frequency oscillating flux: Because of the unsteady nature of the impinging jet, the heat rate can fluctuate rapidly with a large amplitude. Therefore, a hypothetical flux with a sinusoidal distribution will be examined. The Nyquist assumption limits the highest frequency we can recover to be half the sampling rate or f_n = 10 kHz in this case. Two distributions

are examined, $f_n/2$ = 5000 Hz and $f_n/8$ = 1250 Hz, which represent one-half and one-eighth the Nyquist frequency, respectively.

IV. Results

We can quantitatively describe the performance of the different routines under different situations by comparing the rms errors and residuals of the estimates for each test case with the actual data in Table 1. The errors are defined as the difference between the actual and estimated fluxes; whereas the residuals are found as the difference between the simulated data and the temperatures found from the forward-conduction solution to the estimated fluxes. From these values it becomes immediately clear that the two inverse methods provided much more accurate estimates than all other methods, except in the case of the errant temperature spike. The explicit regularization method failed here because we purposely did not incorporate a nonconstant variance of temperature measurements for comparison with the regularization method with nonconstant variance. For the case of nonconstant variance, the diagonal of the Ψ matrix was specified such that each term represented the variance of the measurement at that time given as

$$\text{diag}(\Psi) = \sigma_1^2, \sigma_2^2, \sigma_3^2, \ldots \tag{17}$$

With the inclusion of information concerning the measurement errors, the explicit regularization method results are comparable to the regularization technique. That is to say, when the variance of the measurement at the spike is taken into account the error is 0.93 and 5.75 W/cm^2 for the no-noise and noisy cases, respectively (instead of 119.82 and 126.15 W/cm^2 given in Table 1).

For all cases added noise reduces the accuracy of the estimates (but not significantly in most cases). Note, however, that the Kendall–Dixon method and the regularization technique were able to damp the noise better than other methods because of their smoothing. In the case of the regularization technique the amount of optimal smoothing via the regularization parameter was found to be $\alpha = 0.00001$ K^2 m^4/W^2 using the methods described earlier. The Kendall–Dixon method, on the other hand, is not flexible enough to provide accurate estimates where the flux changes significantly. Details of each test case are discussed in the following subsections.

It should be noted that for the numerical solutions the number of node points was determined by first establishing the minimum required nodes to describe accurately the temperature distributions for all imposed fluxes. These direct numerical solutions to the conduction problem were found to agree with the analytic solutions to within four significant digits. The number of nodes was then quadrupled to remove any doubt about the convergence of the temperature distribution. The problem of not being able to resolve the surface flux, as demonstrated by the class 2 methods, even though the temperature distribution is known accurately, will be discussed in the oscillating flux section where it is more appropriate.

Table 1 Root mean square error and residuals for different test cases and data reduction methods

		Test cases				
					Oscillations	
Method	Noise	Step	Pulse	Spike	$f_N/2$	$f_N/8$
		Flux error, W/cm^2				
Class 1						
Cook–Felderman	0	65.64	24.01	76.79	108.29	42.80
	n	69.33	27.51	80.42	110.65	47.58
Kendall–Dixon	0	141.21	61.78	5.59	337.27	290.11
	n	141.18	79.66	5.67	337.27	290.12
Class 2						
Finite difference	0	35.38	20.88	77.93	93.14	38.43
	n	42.35	24.64	81.69	96.05	44.08
Simple implicit	0	36.22	38.34	55.40	143.54	43.86
	n	41.92	38.93	57.78	145.11	47.36
Rae–Taubee	0	75.92	26.45	72.54	116.60	50.19
	n	78.87	29.09	75.90	118.73	54.18
Class 3						
Regularization	0	28.97	9.11	0.05	21.12	8.78
	n	32.41	18.67	5.11	36.67	19.63
Explicit regularization	0	5.45	6.93	119.82	18.42	4.11
	n	37.64	26.51	126.15	37.74	33.58
		Temperature residual, K				
Class 1						
Cook–Felderman	0	7.15	0.83	1.22	2.84	2.33
	n	7.14	0.90	1.27	2.81	2.37
Kendall–Dixon	0	9.00	2.85	2.59	7.34	13.59
	n	9.01	2.98	2.70	7.38	13.61
Class 2						
Finite difference	0	3.77	0.68	1.11	2.52	2.11
	n	3.77	0.75	1.17	2.53	2.12
Simple implicit	0	1.96	1.16	1.50	3.47	2.56
	n	1.96	1.25	1.57	3.49	2.58
Rae–Taubee	0	8.44	0.83	1.23	5.02	4.95
	n	8.44	0.90	1.29	5.03	4.96
Class 3						
Regularization	0	0.96	0.49	4.71	0.47	0.45
	n	1.05	0.57	4.86	0.47	0.57
Explicit regularization	0	0.13	0.18	0.34	0.35	0.17
	n	0.16	0.20	0.36	0.36	0.18

Note: 0, without noise; n, with noise.

A. Step Flux

Because of the inherent sensitivity of the problem, the Cook–Felderman technique overestimated the step flux at the singularity as shown in Fig. 2. Furthermore, the actual constant flux section was never resolved exactly. A persistent deviation of the estimate from the actual flux can be attributed to the constant property assumption, despite the addition of the correction factor β', suggested by Hollis.[16] The correction factor is only effective for cases with similar temperature histories as those used to generate the correction. Because our case is unusual in this sense and because we did not have adequate data to recreate the correction factor, a marked deviation of the estimate is seen. The Kendall–Dixon method, because of the broad differencing scheme, could not capture the step; there is a slow ramp up to the nominal value when the flux was turned on, and a slow ramping back to zero when the flux was turned off.

A numeric approach to the problem typified by the class 2 methods provided better modeling and, hence, better estimates as noted in Table 1. As expected, the Rae–Taubee technique overestimated the flux at early time steps because of its enhanced grid at early times; but lost its ability to accurately describe the flux at later times. (This will be identified in the oscillating flux section.) Because the finite difference and the simple implicit technique employ fixed grids, they did not resolve the step in flux instantaneously. However, we did note that the estimates tended to become more accurate with time.

The inverse technique contains some features of both classes of techniques. Like class 1 techniques, the inverse methods tended to exaggerate the flux at the singularities. In the regularization method, by using future time steps, a stabilization is introduced in this case that smoothed the capturing of the singularity so it looks more like the Kendall–Dixon method at the singularity. The explicit regularization technique shown in Fig. 2 displays a slight exaggeration at the singularity, but demonstrates agreement throughout the remainder of the experiment. It should be noted, however, that the magnitude of exaggeration and amount of smoothing for class 3 techniques is far less than that of any other technique (see Table 1).

B. Pulse Flux

The pulse estimates are either exaggerated (Cook–Felderman method), fall short (all class 2 methods), or are overly smoothed (Kendall–Dixon method), except for the inverse methods that estimated the actual flux with remarkable accuracy as indicated in Table 1. Here we expect the estimates for all but the regularization method to be the same through the time step that includes the pulse. At the point of the pulse, though, we can determine how the methods are influenced by temperature changes. The inverse methods were able to estimate the nominal value within 5% at the time of the pulse, whereas the next closest estimate (finite difference) was 20% away as seen in Fig. 3a. Not shown is the rebound effect that most methods (other than finite difference) exhibit immediately after the pulse. Compared to the inverse techniques, some methods display a pronounced "ringing" of the estimate in the downstream solution.

C. Temperature Spike

Additional information can be obtained from the zero flux of the spike case that contains measurement errors in the form of background noise and an errant spike. We would like the estimate of the flux to be zero, which we know will not be the case except for the inverse methods that include nonconstant variance of measurement errors and appropriate levels of stabilization. Because we can assume that the variance of the measurement errors is not constant for the regularization method [Ψ^{-1} in Eq. (14)], the errant spike disappeared from the estimate, thereby restoring the actual flux. All other estimates compensated for the errant temperature by estimating a corresponding negative flux immediately after the error as a result of trying to conserve energy (Cook–Felderman in Fig. 3b). Some methods propagated this compensation further, destroying the estimates later in time. Note that the explicit regularization method can also incorporate nonconstant variance of errors, whose unreported results with the nonconstant variance are similar to those of the regularization technique. The results shown in Table 1 are without this feature to draw a comparison to methods that cannot include this information.

As an example of how measurements become exaggerated during the estimation process, we can revisit Fig. 3b. Notice that while the variance of the noise is 0.32 K^2, which is only 0.02% of the nominal temperature rise, the magnitude of the fluctuations because of noise is approximately ± 30 W/cm^2, which is roughly 3% of our nominal flux (Fig. 3c).

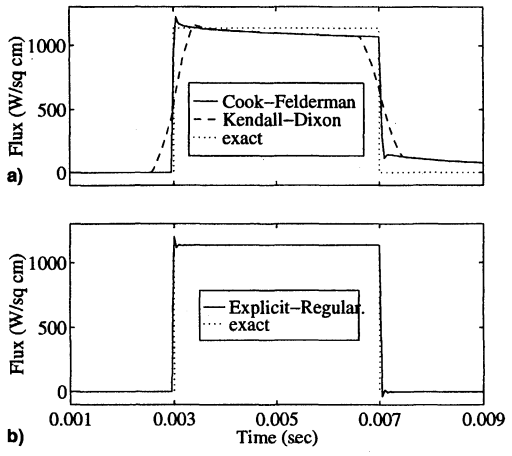

Fig. 2 Step test case: a) the class 1 techniques miss the actual flux because of temperature-dependent properties, whereas the b) explicit regularization provided the most accurate estimation.

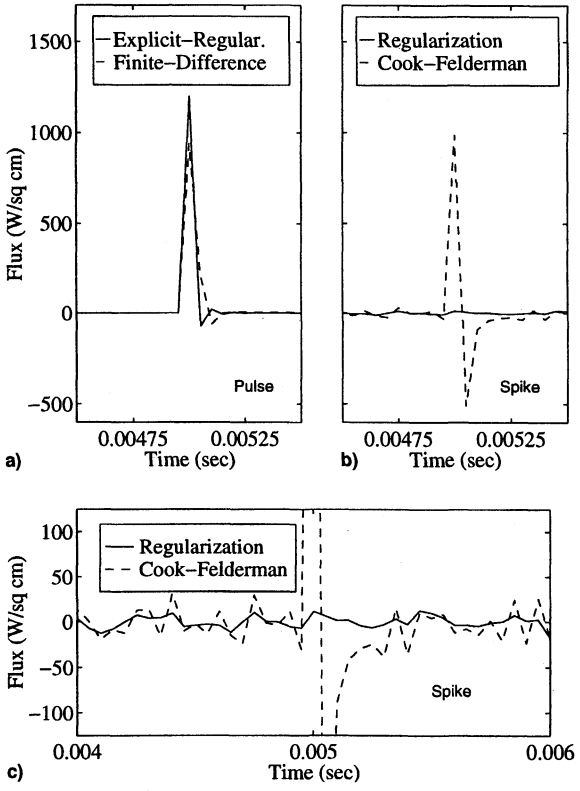

Fig. 3 a) Pulse and b) and c) spike. The inverse methods (explicit regularization in the a) and regularization in b) and c), demonstrate the ability to more accurately model the pulse and reduce the influence of noise compared to traditional techniques.

D. High-Frequency Oscillating Flux

High-frequency fluxes tend to introduce new concerns about the estimation methods. Firstly, we can run into modeling problems at high frequencies. Most estimation methods assume that the flux is piecewise constant over time. The finite element code used to generate the temperature data, however, more accurately assumes a piecewise linear distribution between time steps (see Fig. 4). Even though the integral of both histories may be the same, the resulting temperature distributions will not be similar, particularly at the surface where the measurements occur. This influence, however, is less apparent at lower frequencies. As expected, all methods provided a better estimates as the frequency of the oscillations decreased.

No class 1 or 2 methods could resolve the magnitude of the oscillations in both high-frequency cases. Even those methods that by nature exaggerate the actual flux were not able to capture the actual amplitude. This is an artifact of the piecewise constant assumption. A constant flux at a given magnitude adds much more energy than a linearly varying flux from zero to the designated magnitude. To illustrate this, notice Fig. 4 where one cycle of our assumed flux is compared with the two types of approximations used. We notice that for coarse time steps relative to the frequency, the piecewise constant approximation cannot resolve the true nature of the flux. Therefore, the methods compensated by estimating a lower flux than the actual flux at a given time. This can be seen from the Cook–Felderman method in Fig. 5. The Kendall–Dixon method on the other hand contains so much smoothing that the high-frequency components were virtually lost (also in Fig. 5). Notice that the estimate converged to the average flux of 568 W/cm^2 (500 Btu/ft^2 s), thus conserving energy.

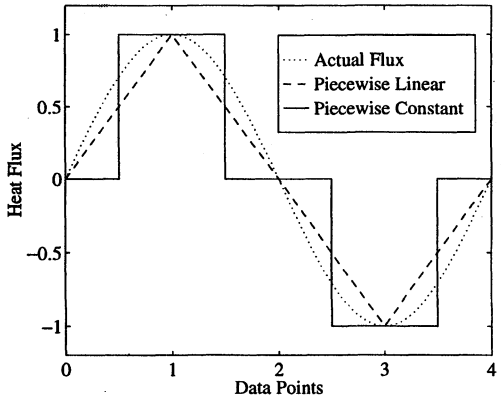

Fig. 4 Piecewise constant approximation contains gross errors compared to the piecewise linear approximation for high-frequency components.

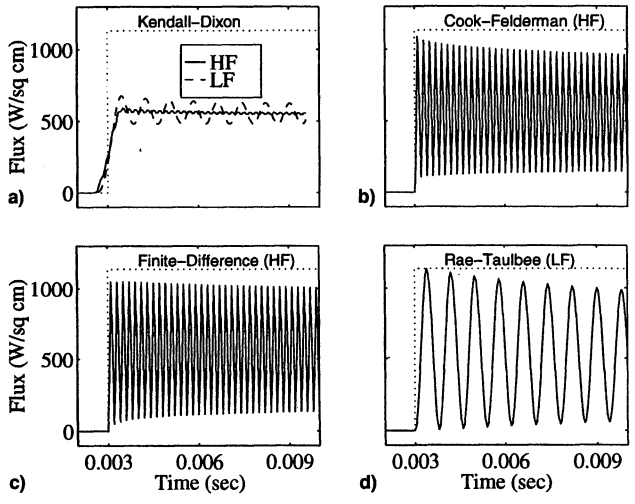

Fig. 5 High- and low-frequency oscillation test cases (HF and LF, respectively). These plots show the oversmoothing of the a) Kendall–Dixon method, b) the piecewise linear assumption of the Cook–Felderman, c) the lack of spatial resolution of the finite difference and d) the slow decay of resolution in the Rae–Taubee.

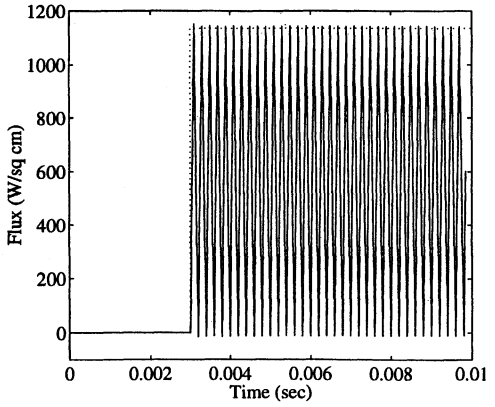

Fig. 6 High-frequency oscillating test case. The regularization technique was able to estimate the magnitude of the extrema most accurately, overcoming the problems associated with other methods.

Class 2 methods, however, can approach a linear distribution by taking progressively smaller calculation time steps until the piecewise constant distribution for each time step looks like the linear distribution. However, these methods could not resolve the steep temperature gradient accurately and fell short of the actual flux. The finite difference method, which can calculate the surface flux more accurately because of the inclusion of the storage term, still failed to find the flux accurately as in Fig. 5. The Rae–Taubee method on the other hand demonstrates relatively accurate estimates at early times. Because of the stretched grid, however, later estimates fell short as demonstrated by the low-frequency case (Fig. 5).

Note that both inverse techniques provided excellent estimates for both the low-frequency and the more difficult high-frequency cases as noted in Table 1, which gives the rms errors and residuals. The ability of the regularization method to capture the magnitude of the flux throughout the experiment can also be seen in Fig. 6.

E. Summary

In summarizing the results of this analysis, we can qualitatively describe the capabilities of each technique in response to different features or data characteristics highlighted by the various test cases as shown in Table 2. Here it can be seen that in the class 1 methods, the Kendall–Dixon method outperformed the Cook–Felderman method in handling data noise at the expense of oversmoothing the data in the cases where the flux changed rapidly. Class 2 methods were prone to either under or overestimating the response, while class 3 methods provided the best agreement overall. The drawbacks of the class 1 methods can largely be attributed to its inability to model the physics adequately; however, the fundamental weaknesses of the class 2 methods are not as apparent.

Throughout this analysis we have stated that even though the temperature distribution is converged, we cannot accurately determine the gradient at the surface from this distribution. This is best seen when we examine high-frequency oscillating fluxes. We must realize that there is another time scale present: The penetration depth of the flux for the current time step. The penetration of a flux at a given time step is inversely proportional to the sample rate or proportional to the time between measurements. We must accurately resolve the temperature distribution over this penetration depth, which is typically much smaller than the node spacing required to produce a converged temperature solution. As the node spacing decreases, a better estimate can be obtained. The size of the problem, however, becomes undesirable. It was found that for most

Table 2 Qualitative evaluation of specific data characteristics for different classes of methods

Method	Characteristics in data						
	Simulated experimental noise	Large errant temperature spike	Short, high-magnitude flux	Large temperature change	Oscillating flux	Constant flux	Historical accuracy
Class 1							
Cook–Felderman	e	x	m	e	m	g	n
Kendall–Dixon	g	g	x	s	x	g	n
Class 2							
Finite difference	e	x	s	e	s	g	l
Rae–Taubee	e	x	s	e	s	x	i
Simple implicit	e	x	s	s	s	g	l
Class 3							
Regularization	g	g	g	g	g	g	n
Explicit regularization	e	x[a]	g	g	g	g	n

Note: e, exaggeration because of sensitivity of the flux to temperature; x, unacceptable agreement; m, under estimate due to modeling; g, good agreement; s, under estimate because of gradient calculation at the surface; l, later time agreement; i, initial time agreement; and n, not affected.

[a]With inclusion of nonconstant variances this designation is g.

cases we needed aminimum of 1000 node points for class 2 techniques to approach the accuracy of the inverse solution that required only 20 nodes. (Keep in mind that this is a one-dimensional problem.) The necessary integration time steps then increased with the square of the number of nodes. As a result, we have a computationally enormous problem that still cannot resolve the flux as accurately as we would like. Because the inverse techniques are not constrained to finding this numerical derivative of the distribution, we must concern ourselves with resolving the surface temperature only, which is much simpler.

V. Conclusions

It has become apparent that an inverse method is the most stable and accurate of the methods examined for a completely unknown flux. It is important to note that the class 3 methods are more robust in every situation examined. In general, the class 1 techniques exaggerate temperature changes and the class 2 techniques cannot model the large gradients. Additional advantages of the inverse technique include the statistical elimination of experimental noise, increased stability of the solution, extendibility to multidimensional problems, and the inclusion of other known information such as the variance of measurement errors and sensor modeling.

Despite the overwhelming advantages of accuracy and stability, the drawbacks of the inverse technique are that the appropriate amount of stabilization must be determined before analysis, and that computation is roughly four times that of the numerical techniques when using the same number of nodes. However, as previously discussed, class 2 methods can require 50 times the number of nodes to resolve the heat flux with the same accuracy as the inverse methods. Note that all analyses were on the order of seconds on a 90-MHz Pentium.

The lack of accuracy of the class 1 methods stems from the fact that they are limited in their ability to model the physics adequately. Class 2 methods can model the physics, but are restricted in their ability to resolve surface gradients. In other words, the numerical derivative at the surface can not be modeled sufficiently even though the temperature distribution from the conduction analysis is correct. By employing an inverse technique, we can model the physics accurately, eliminate the need to find temperature gradients, and introduce stabilization for noisy data to allow more accurate estimates than can be obtained with class 1 or 2 techniques.

Acknowledgments

The authors thank Robert Nowak, Research Scientist, at NASA Langley Research Center for his help in determining the relevance and practicality of this research. We would also like to thank the NASA Langley Research Center for awarding a Graduate Student Research Program Fellowship, NGT-51249, which made this work possible.

References

[1]Watts, J., "Flight Experience with Shock Impingement and Interface Heating on the X-15-2 Research Airplane," NASA TR, TM X-1669, Oct. 1968.

[2]Burcham, F., Jr., and Nugent, J., "Local Flow Field Around a Pylon-Mounted Dummy Ramjet Engine on the X-15-2 Airplane for Mach Numbers from 2.0 to 6.7," NASA TN D-5638, Feb. 1970.

[3]Edney, B., "Shock Interference and the Space Shuttle," NASA TR, TM X-52876, July 1970.

[4]Hiers, R., and Loubsky, W., "Effects of Shock-Wave Impingement on the Heat Transfer on a Cylindrical Leading Edge," NASA TN D-3859, Feb. 1967.

[5]Gladden, H. J., and Mellis, M., "Hypersonic Engine Leading Edge Experiments in a High Heat Flux, Supersonic Flow Environment," NASA TM 106742, Winter Meeting of the American Society of Mechanical Engineers, Nov. 1994.

[6]Holden, M., Wieting, A., Moselle, J., and Glass, C., "Studies of Aerothermal Loads Generated in Regions of Shock/Shock Interaction in Hypersonic Flow," AIAA Paper 88-0477, Jan. 1988.

[7]Holden, M., Moselle, J., and Lee, J., "Studies of Aerothermal Loads Generated in Regions of Shock/Shock Interaction in Hypersonic Flow," NASA CR 181893, Oct. 1991.

[8]Berry, S., and Nowak, R., "Effects of Fin Leading Edge Sweep on Shock-Shock Interaction at Mach 6," AIAA Paper 96-0230, Jan. 1996.

[9]Seymour, P. J., "Techniques for Numerical Evaluation of Unsteady Heat Flux From Thin Film Gauges," MS Thesis, State Univ. of New York, Buffalo, NY, 1987.

[10]Beck, J., Blackwell, B., and St. Clair, C., Jr., Inverse Heat Conduction: *Ill-Posed Problems*, Wiley, New York, 1985.

[11]Ehrich, F. F., "Differentiation of Experimental Data Using Least Squares Fitting," *Journal of Aeronautical Sciences*, Feb. 1954, pp. 133, 134.

[12]Vidal, R. J., "Model Instrumentation Techniques for Heat Transfer and Force Measurements in a Hypersonic Shock Tunnel," Cornell Aeronautic Lab., Rept. AD-917-A-1, Cornell Univ., NY, Feb. 1956.

[13]Schultz, D. L., and Jones, T. V., "Heat Transfer Measurements in Short Duration Hypersonic Facilities," AGARDograph, TR 165, Feb. 1973.

[14]Cook, W. J., and Felderman, E. J., "Reduction of Data from Thin Film Heat Transfer Gages: A Concise Numerical Technique," *AIAA Journal*, Vol. 4, No. 3, 1966, pp. 561–562.

[15]Cook, W. J., "Unsteady Heat Transfer to a Semi-Infinite Solid with Arbitrary Surface Temperature History and Variable Thermal Properties," Engineering Research Inst., Iowa State Univ., TR ISU-ERI-Ames 67500, Ames, IA, 1970.

[16]Hollis, B. R., "User's Manual for the One-Dimensional Hypersonic Experimental Aero-Thermodynamic (1DHEAT) Data Reduction Code," NASA CR 4691, Aug. 1995.

[17]Kendall, D. N., and Dixon, W. P., "Heat Transfer Measurements in a Hot Shot Wind Tunnel," *Transactions on Aerospace and Electronic Systems*, Vol. AES-3, No. 4, 1996, pp. 596–603.

[18]Hedlund, E. R., Hill, F. A. F., Ragsdale, W. C., and Voisinet, R. L. P., "Heat Transfer Testing in the NSWC Hypervelocity Wind Tunnel Utilizing Co-Axial Surface Thermocouples," MP 80-15I, NSWC, Dahlgren, VA, March 1980.

[19]Cook, W. J., "Determination of Heat Transfer Rates from Transient Surface Temperature Measurements, *AIAA Journal*, Vol. 8, No. 7, 1970, pp. 1366–1368.

[20]Patankar, S. V., *Numerical Heat Transfer and Fluid Flow*, Taylor and Francis, Washington, DC, 1980.

[21]Dunn, M. G., George, W. K., Rae, W. J., Woodward, S. H., Moller, J. C., and Seymour, P. J., "Heat Flux Measurements for the Rotor of a Full-Stage Turbine: Part II: Description of Analysis Technique and Typical Time-Resolved Measurements," *Journal of Turbomachinery*, Vol. 108, No. 1, 1986, pp. 98–107.

[22]Glass, C. E., "Experimental Study of Pressure and Heating Rate on a Swept Cylindrical Leading Edge Resulting from Swept Shock Wave Interference," MS Thesis, Old Dominion Univ., Norfolk, VA, April 1989.

[23]Holden, M. S., and Kolly, J. M., "Measurements of Heating in Regions of Shock/Shock Interaction in Hypersonic Flow," AIAA Paper 95-0640, Jan. 1995.

[24]George, W. K., Rae, W. J., and Woodward, S. H., "An Evaluation of Analog and Numerical Techniques for Unsteady Heat Transfer Measurements with Thin Film Gauges in Transient Facilities," *Experimental Thermal and Fluid Science*, Vol. 4, 1991, pp. 333–342.

[25]Walker, D. G., and Scott, E. P., "One-Dimensional Heat Flux History Estimation from Discrete Temperature Measurements," American Society of Mechanical Engineers International Symposium and Exposition, San Francisco, CA, Nov. 1995.

[26]Tikhonov, A. N., and Arsenin, V. Y., *Solutions of Ill-Posed Problems*, V. H. Winston and Sons, Washington, DC, 1977.

[27]Scott, E., and Beck, J., "Analysis of Order of the Sequential Regularization Solutions of Inverse Heat Conduction Problems," *Journal of Heat Transfer*, Vol. 111, May 1987, pp. 218–224.

[28]Beck, J. V., "Criteria for Comparison of Methods of Solution of the Inverse Heat Conduction Problem," *Nuclear Engineering and Design*, Vol. 53, 1979, pp. 11–22.

[29]Murio, D. A., "On the Characterization of the Solution of the Inverse Heat Conduction Problem," American Society of Mechanical Engineers, *Winter Annual Meeting*, Miami Beach, FL, Nov. 1985.

[30]Trucco, R. E., and Tamango, J., "Elimination of an External Noise Spike on the Thin Film Temperature Traces," General Applied Science Lab., TM 240, Long Island, NY, June 1990.